Supplementary materials for：

Mitigation of Gilbert damping in the CoFe/CuO_x orbital torque system

Shilei Ding*, Hanchen Wang, William Legrand, Paul Noël, Pietro Gambardella*

Department of Materials, ETH Zürich, 8093 Zürich, Switzerland

Table of contents

S1. Surface roughness

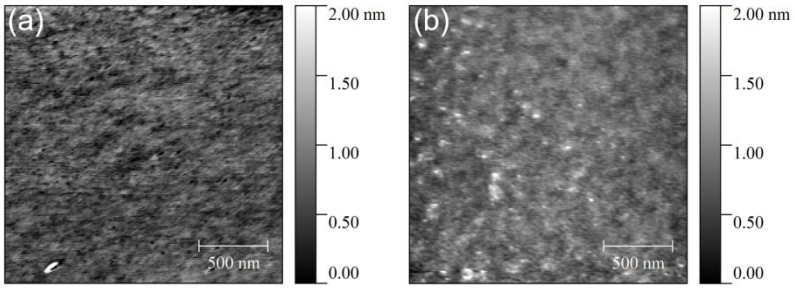

Figure S1. Atomic force microscopy images of (a) CoFe(3)/Pt(5) and (b) CoFe(3)/CuO_x(5).

The CoFe(t_{CoFe})/CuO_x(5) samples were exposed to air for at least 2 days before starting the electrical measurements. We used atomic force microscopy (AFM) to investigate their surface roughness. Figure S1(a) and (b) show the AFM images of CoFe(3)/Pt(5) and CoFe(3)/CuO_x(5). Surface grains appear to form in the CoFe(3)/CuO_x(5) sample, after the partial oxidization of Cu.

The root mean square roughness is 0.2 nm for CoFe(3)/CuO_x(5), indicating a relatively flat surface.

S2. Anomalous Hall and planar Hall effect measurements

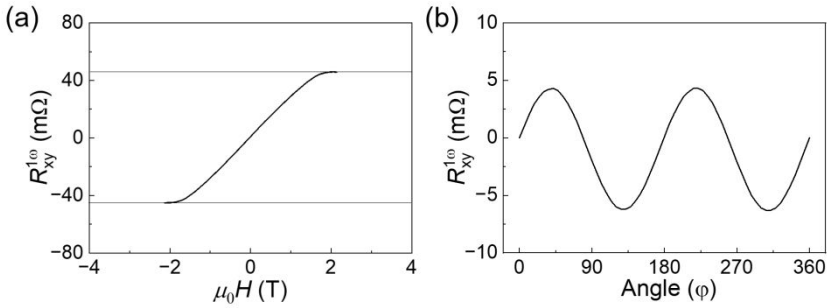

Figure S2. (a) Anomalous Hall resistance of CoFe(3)/CuO_x(5) as a function of out-of-plane magnetic field. (b) Planar Hall resistance of CoFe(3)/CuO_x(5) as a function of the angle between external field and current. The external field was set to 1.4 T. The applied current is 1 mA in both cases.

Figure S2(a) shows the anomalous Hall resistance of CoFe(3)/CuO_x(5) with the applied current of 1 mA, from which we obtain the anomalous Hall coefficient $R_{\mathrm{AHE}} = 45\ \mathrm{m\Omega}$ and $\mu_0 H_{\mathrm{dem+ani}} = 1.7\ \mathrm{T}$, which is mostly due to the demagnetization and anisotropy field. We also measure the planar Hall coefficient R_{PHE}, as required for the measurement of the SOT by the harmonic Hall voltage method. We obtain $R_{\mathrm{PHE}} = 5.3\ \mathrm{m\Omega}$ by fitting the angular dependence of the planar Hall resistance, as shown in Figure S2(b).

S3. Saturation magnetization

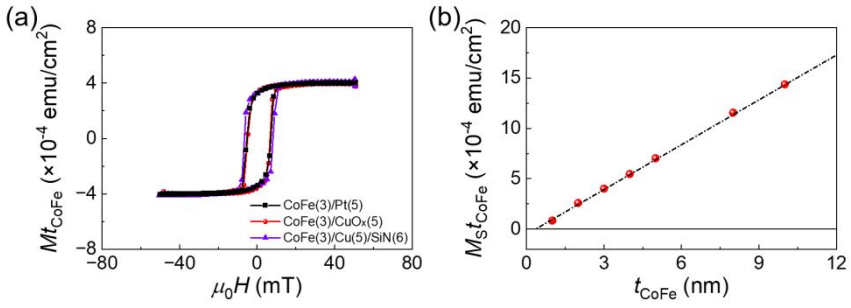

Figure S3. (a) Magnetization loops of CoFe samples with different overlayers measured by SQUID. (b) Thickness dependence of the areal saturation magnetization in CoFe(t_{CoFe})/CuO_x(5).

Figure S3(a) shows the hysteresis loops of the CoFe samples with different overlayers measured by a superconducting quantum interference device (SQUID) as a function of in-plane magnetic field. The different overlayers do not affect the saturation magnetization of CoFe in a significant way. Figure S3(b) presents the areal saturation magnetization of CoFe(t_{CoFe})/CuO_x(5) as a function of CoFe thickness. From the intercept of the linear fit with the *x* axis, we determine the presence of a magnetic dead layer with a thickness of about 0.4 nm.

S4. Longitudinal resistance of CoFe(t_{CoFe})/Pt(5) and CoFe(t_{CoFe})/CuO_x(5)

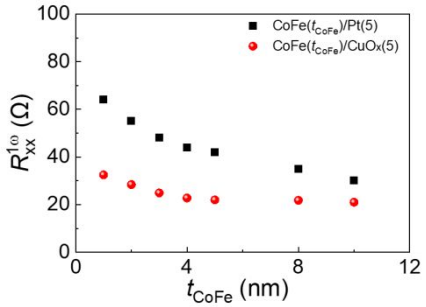

Figure S4. Longitudinal resistance of CoFe(t_{CoFe})/Pt(5) and CoFe(t_{CoFe})/CuO_x(5) as a function of CoFe thickness. The CoFe/CuO_x samples have a lower resistance compared to CoFe/Pt due to the low resistivity of unoxidized Cu in CuO_x.

Figure S4 shows the resistance of the CoFe(t_{CoFe})/Pt(5) and CoFe(t_{CoFe})/CuO_x(5)sample series as a function of CoFe thickness. From the resistance R, we calculate the electric field as $E = I_0 R/L$, where I_0 is the peak amplitude of the ac current and L the distance between the resistance contacts. This expression is used for the calculation of the damping-like torque efficiency per unit applied electric field as we discussed in the main text and the section S5.

S5. Hamonic Hall voltage measurements of the damping-like and field-like SOT

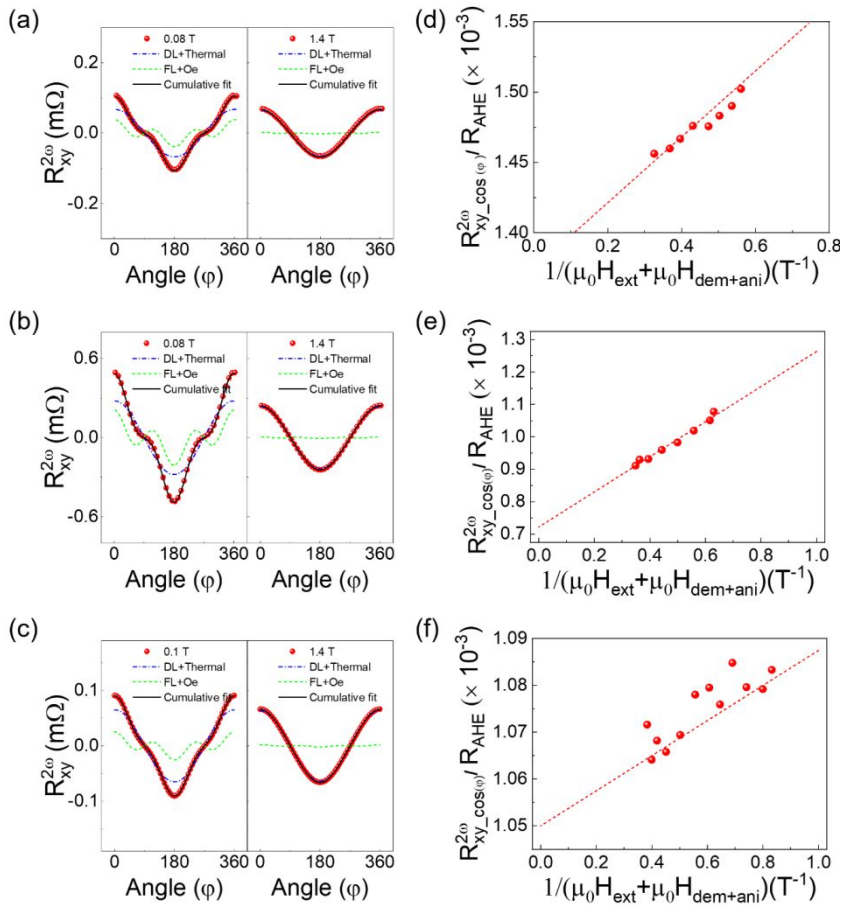

Figure S5. (a,b,c) Transverse second harmonic resistance $R_{xy}^{2\omega}(\varphi)$ of CoFe(3)/CuO$_x$(5), CoFe(3)/Pt(5) and CoFe(3)/Cu(5)/SiN(6) as a function of the in-plane angle φ between applied magnetic field and current. The applied currents are 18, 9, and 17 mA respectively. (d,e,f) $R_{xy\_cos(\varphi)}^{2\omega}/R_{AHE}$ as a function of $(\mu_0 H_{ext} + \mu_0 H_{dem+ani})^{-1}$ for an applied current of amplitude $I_0 =$ 18, 9, and 17 mA for CoFe(3)/CuO$_x$(5), CoFe(3)/Pt(5) and CoFe(3)/Cu(5)/SiN(6), respectively.

The orbital torque has a different origin in comparison to the spin torque, however, they share the same symmetry [1]. Thus, the method for spin torque detection is also valid for the orbital torque. When applying an ac current $I(t) = I_0 \cos(2\pi f_1 t)$ through the Hall bar (as shown in Figure 1(b) in the main text), the current-induced torque leads to the periodic oscillation of the magnetization, which modulates the Hall voltage at the same frequency as the ac current, giving rise to a second-harmonic Hall resistance. The dependence of the second-harmonic resistance $R_{xy}^{2\omega}(\varphi) = V_{xy}^{2\omega}(\varphi)/I_0$ on the angle φ between the magnetization and the current direction (x-axis) can be expressed as [2,3]:

$$R_{xy}^{2\omega}(\varphi) = \left(\frac{1}{2} R_{AHE} \frac{\mu_0 H_{DL}}{\mu_0 H_{ext} + \mu_0 H_{dem+ani}} + R_{\nabla T}\right)\cos(\varphi) + R_{PHE}(2\cos^3(\varphi) - \cos(\varphi)) \frac{\mu_0 H_{FL} + \mu_0 H_{Oe}}{\mu_0 H_{ext}}. \quad s(1)$$

Here R_{AHE} is the anomalous Hall resistance, $\mu_0 H_{DL}$ and $\mu_0 H_{ext}$ represent the damping-like torque effective field and the applied magnetic field, respectively, and $\mu_0 H_{dem+ani}$ the effective magnetic anisotropy field due to the sum of demagnetizing field and magnetocrystalline anisotropy. $R_{\nabla T}$ is the thermal resistance including the anomalous Nernst effect and the spin Seebeck effect

from the temperature gradient ∇T. R_{PHE} is the planar Hall resistance. $\mu_0 H_{\mathrm{FL}}$ and $\mu_0 H_{\mathrm{Oe}}$ stand for the effective field from the field-like torque and the Oersted field, respectively; the latter can be estimated via Ampère's law. In the CoFe(3)/CuO_x(5) sample at room temperature, we have $R_{\mathrm{AHE}} = 45\ \mathrm{m\Omega}$, $\mu_0 H_{\mathrm{dem+ani}} = 1.7\ \mathrm{T}$ and $R_{\mathrm{PHE}} = 5.3\ \mathrm{m\Omega}$ (Section S2). Figure S5(a) shows the angular dependence of $R_{\mathrm{xy}}^{2\omega}(\varphi)$ for CoFe(3)/CuO_x(5) in a weak and strong magnetic field. By fitting the curves measured for different field strengths with Eq. s(1), we separate the $\cos(\varphi)$ part of the second harmonic resistance $R_{\mathrm{xy\_cos}(\varphi)}^{2\omega}$, which depends on the damping-like torque. Figure S5(d) shows that $R_{\mathrm{xy\_cos}(\varphi)}^{2\omega}/R_{\mathrm{AHE}}$ scales linearly with $1/(\mu_0 H_{\mathrm{ext}} + \mu_0 H_{\mathrm{dem+ani}})$, which gives $\mu_0 H_{\mathrm{DL}} = 0.35 \pm 0.04\ \mathrm{mT}$ for a current of amplitude $I_0 =$ 18 mA. Similarly, we found $\mu_0 H_{\mathrm{DL}} = 1.02 \pm 0.06\ \mathrm{mT}$ for CoFe(3)/Pt(5) with a current of amplitude $I_0 =$ 9 mA from Figure S5(b) and (e) and $\mu_0 H_{\mathrm{DL}} = 0.07 \pm 0.02\ \mathrm{mT}$ for CoFe(3)/Cu(5)/SiN(6) with a current of amplitude $I_0 =$ 17 mA from Figure S5(c) and (f). One can further vary the applied current, and obtain the electric field dependence of the effective damping-like torque field as shown in Figure 1(c) in the main text. The electric field is calculated as explained in Section S4.

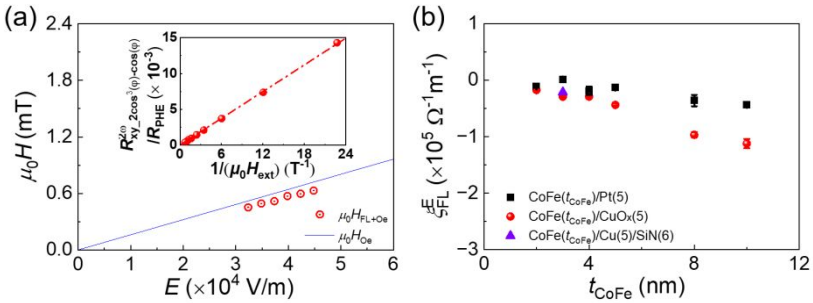

Figure S6. (a) $\mu_0 H_{\mathrm{FL}} + \mu_0 H_{\mathrm{Oe}}$ of CoFe(3)/CuO_x(5) as a function of applied electric field. The blue dashed line shows the estimated Oersted field. The inset shows $R_{\mathrm{xy\_}2\cos^3(\varphi)-\cos(\varphi)}^{2\omega}/R_{\mathrm{PHE}}$ as a function of $1/\mu_0 H_{\mathrm{ext}}$, for an applied current of amplitude I_0 = 18 mA. (b) Field-like torque efficiency as a function of the CoFe thickness in CoFe(t_{CoFe})/Pt(5) and CoFe(t_{CoFe})/CuO_x(5).

The field-like torque efficiency can be obtained from the analysis of the $2\cos^3(\varphi) - \cos(\varphi)$ component of the second harmonic resistance in Eq. s(1), $R_{\mathrm{xy\_}2\cos^3(\varphi)-\cos(\varphi)}^{2\omega}$. The inset of Figure S6(a) shows $R_{\mathrm{xy\_}2\cos^3(\varphi)-\cos(\varphi)}^{2\omega}/R_{\mathrm{PHE}}$ as a function of $1/\mu_0 H_{\mathrm{ext}}$ for CoFe(3)/CuO_x(5). From the slope of this curve, we obtain the total field $\mu_0 H_{\mathrm{FL}} + \mu_0 H_{\mathrm{Oe}}$. The results of several measurements of $\mu_0 H_{\mathrm{FL}} + \mu_0 H_{\mathrm{Oe}}$ as a function of the applied electric field are shown in Figure S6(a). The Oersted field can be estimated as $\mu_0 H_{\mathrm{Oe}} = \frac{I_0}{2\pi}$ -> 0.04 mT/mA (blue line). By subtracting the Oersted field, we calculate the efficiency of the field-like torque as

$$\xi_{\mathrm{FL}}^{\mathrm{E}} = \frac{\frac{2e}{\hbar} M_s t_{\mathrm{CoFe}} \mu_0 H_{\mathrm{FL}}}{E}.$$

Figure S6 (b) shows the dependence of $\xi_{\mathrm{FL}}^{\mathrm{E}}$ on thickness of CoFe in the CoFe(t_{CoFe})/Pt(5) and CoFe(t_{CoFe})/CuO_x(5) series. The field-like torque slightly increases in magnitude in

CoFe(t_{CoFe})/CuO_x(5) as a function of CoFe thickness. We remark, however, that a precise estimate of $\xi^{\mathrm{E}}_{\mathrm{FL}}$ is challenging because the distribution of the current in these samples can vary as a function of thickness, thus affecting the calculation of the Oersted field.

S6. Torque to damping ratios

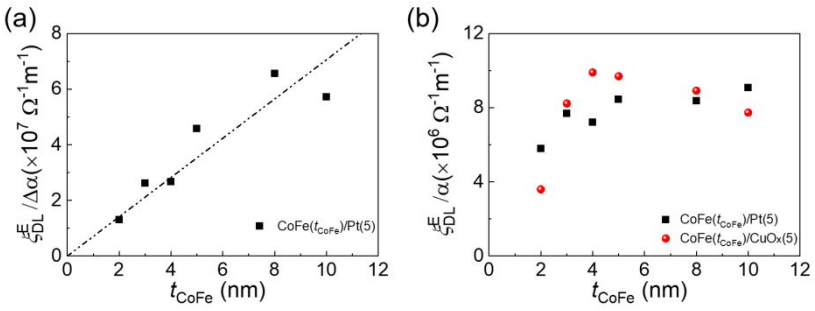

Figure S7. (a) $\xi^{\mathrm{E}}_{\mathrm{DL}}/\Delta\alpha$ as a function of CoFe thickness. The dash-doted line is a linear fit by Eq. s(4). (b) $\xi^{\mathrm{E}}_{\mathrm{DL}}/\alpha$ as a function of CoFe thickness in CoFe(t_{CoFe})/Pt(5) and CoFe(t_{CoFe})/CuO_x(5).

As we discussed in the main text, in a purely spin torque system, spin pumping leads to the enhancement of the damping parameter. The phenomenological damping is $\alpha = \alpha_0 + \Delta\alpha$ where $\Delta\alpha$ can be expressed as [4]

$$\Delta\alpha = \frac{\gamma\hbar}{4\pi M_s t_{\mathrm{CoFe}}} g^{\uparrow\downarrow}. \qquad \text{s(2)}$$

We recall that Eq. s(2) assumes that the thickness of the nonmagnetic layer is thicker than the spin diffusion length, leading to a negligible spin-back flow.

In the linear response limit, the Onsager relations predict a reciprocal relationship between the torque and spin pumping efficiencies. In the standard drift-diffusion approach [5] and neglecting spin backflow, the damping-like SOT efficiency per unit applied electrical field is given approximately by [6]

$$\xi^{E}_{DL} = \frac{2e^2}{h} g^{\uparrow\downarrow} \lambda_N \rho_N \sigma_S, \qquad \text{s(3)}$$

where h is the plank constant, $g^{\uparrow\downarrow}$ the effective spin mixing conductance of the FM/NM interface, and ρ_N, and σ_S are the resistivity and spin Hall conductivity of the NM, respectively. Combining Eqs. s(2) and s(3), one obtains:

$$\frac{\xi^{\mathrm{E}}_{\mathrm{DL}}}{\Delta\alpha} = \frac{4e^2}{\gamma\hbar^2} \lambda_N \rho_N \sigma_S M_s t_{\mathrm{CoFe}}. \qquad \text{s(4)}$$

Thus, we expect $\xi^{\mathrm{E}}_{\mathrm{DL}}/\Delta\alpha \sim M_s t_{\mathrm{CoFe}}$, as indeed shown in Figure S7(a) for the CoFe(t_{CoFe})/Pt(5) series.

The above reasoning fails for an orbital torque system, as $\Delta\alpha$ remains close to zero over the entire range of CoFe thicknesses in CoFe(t_{CoFe})/CuO_x(5). We can nonetheless plot the ratio between

torque efficiency and the total damping for the two sample series, namely ξ_{DL}^{E}/α as a function of CoFe thickness, as shown in Figure S7(b). Even when considering the contributions to damping that are not due to angular momentum pumping, our data indicate that an orbital torque system provides a favorable torque-to-damping ratio as the thickness of CoFe exceeds 3 nm.

Supplementary References

1. D. Go and H.-W. Lee, Orbital Torque: Torque Generation by Orbital Current Injection, *Phys. Rev. Res*. **2**, 13177 (2020).
2. K. Garello, I. M. Miron, C. O. Avci, F. Freimuth, Y. Mokrousov, S. Blügel, S. Auffret, O. Boulle, G. Gaudin, and P. Gambardella, Symmetry and Magnitude of Spin-Orbit Torques in Ferromagnetic Heterostructures, *Nat. Nanotechnol.* **8**, 587 (2013).
3. C. O. Avci, K. Garello, M. Gabureac, A. Ghosh, A. Fuhrer, S. F. Alvarado, and P. Gambardella, Interplay of Spin-Orbit Torque and Thermoelectric Effects in Ferromagnet/Normal-Metal Bilayers, *Phys. Rev. B* **90**, 224427 (2014).
4. A. Conca, B. Heinz, M. R. Schweizer, S. Keller, E. T. Papaioannou, and B. Hillebrands, Lack of Correlation between the Spin-Mixing Conductance and the Inverse Spin Hall Effect Generated Voltages in CoFeB/Pt and CoFeB/Ta Bilayers, *Phys. Rev. B* **95**, 174426 (2017).
5. Y. Tserkovnyak, A. Brataas, G. E. W. Bauer, and B. I. Halperin, Nonlocal Magnetization Dynamics in Ferromagnetic Heterostructures, *Rev. Mod. Phys*. **77**, 1375 (2005).
6. C.-F. Pai, Y. Ou, L. H. Vilela-Leão, D. C. Ralph, and R. A. Buhrman, Dependence of the Efficiency of Spin Hall Torque on the Transparency of Pt/Ferromagnetic Layer Interfaces, *Phys. Rev. B* **92**, 64426 (2015).
7. A. Conca, S. Keller, M. R. Schweizer, E. T. Papaioannou, and B. Hillebrands, Separation of the Two-Magnon Scattering Contribution to Damping for the Determination of the Spin Mixing Conductance, *Phys. Rev. B* **98**, 214439 (2018).